

Copyright (2017). This article may be downloaded for personal use only. Any other use requires permission of the author and the American Institute of Physics.

*The following article appeared in (**J. Chem. Phys.**, 147, 241102, 2017) and may be found at (<http://aip.scitation.org/doi/full/10.1063/1.5013253>)*

Communication: Relationship between local structure and the stability of water in hydrophobic confinement

Y. Elia Altabet, and Pablo G. Debenedetti

Citation: *The Journal of Chemical Physics* **147**, 241102 (2017); doi: 10.1063/1.5013253

View online: <https://doi.org/10.1063/1.5013253>

View Table of Contents: <http://aip.scitation.org/toc/jcp/147/24>

Published by the [American Institute of Physics](#)

Articles you may be interested in

[Perspective: Surface freezing in water: A nexus of experiments and simulations](#)

The Journal of Chemical Physics **147**, 060901 (2017); 10.1063/1.4985879

[Temperature-dependent vibrational spectra and structure of liquid water from classical and quantum simulations with the MB-pol potential energy function](#)

The Journal of Chemical Physics **147**, 244504 (2017); 10.1063/1.5006480

[Principal component analysis on a torus: Theory and application to protein dynamics](#)

The Journal of Chemical Physics **147**, 244101 (2017); 10.1063/1.4998259

[Construction of non-Markovian coarse-grained models employing the Mori–Zwanzig formalism and iterative Boltzmann inversion](#)

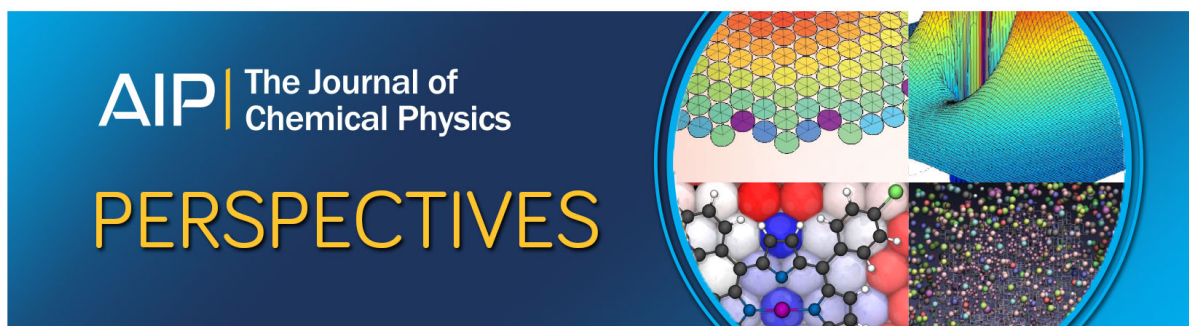
The Journal of Chemical Physics **147**, 244110 (2017); 10.1063/1.5009041

[Communication: Counter-ion solvation and anomalous low-angle scattering in salt-free polyelectrolyte solutions](#)

The Journal of Chemical Physics **147**, 241103 (2017); 10.1063/1.5010784

[Communication: Truncated non-bonded potentials can yield unphysical behavior in molecular dynamics simulations of interfaces](#)

The Journal of Chemical Physics **147**, 121102 (2017); 10.1063/1.4997698



Communication: Relationship between local structure and the stability of water in hydrophobic confinement

Y. Elia Altabet and Pablo G. Debenedetti^{a)}

Department of Chemical and Biological Engineering, Princeton University, Princeton, New Jersey 08544, USA

(Received 12 November 2017; accepted 13 December 2017; published online 28 December 2017)

Liquid water confined between nanoscale hydrophobic objects can become metastable with respect to its vapor at nanoscale separations. While the separations are only several molecular diameters, macroscopic theories are often invoked to interpret the thermodynamics and kinetics of water under confinement. We perform detailed rate and free energy calculations via molecular simulations in order to assess the dependence of the rate of evaporation, free energy barriers, and free energy differences between confined liquid and vapor upon object separation and compare them to the relevant macroscopic theories. At small enough separations, the rate of evaporation appears to deviate significantly from the predictions of classical nucleation theory, and we attribute such deviations to changes in the structure of the confined liquid film. However, the free energy difference between the confined liquid and vapor phases agrees quantitatively with macroscopic theory, and the free energy barrier to condensation displays qualitative agreement. Overall, the present work suggests that theories attempting to capture the kinetic behavior of nanoscale systems should incorporate structural details rather than treating it as a continuum. *Published by AIP Publishing.* <https://doi.org/10.1063/1.5013253>

Performing atomistic simulations to probe nanoscale phenomena is an often useful complement to experimental investigation. However, the results obtained from such computer experiments are then often interpreted using continuum theories that are agnostic to the existence of atoms and molecules, let alone their structural arrangement. While there is no good reason *a priori* to rely on such theories, if continuum descriptions prove successful, they can then serve as convenient tools for engineering design at the nanoscale. The present work explores an example of nanoscale science where macroscopic theories are often invoked.

The specific nanoscale phenomenon we consider is the fact that water confined between hydrophobic objects of sufficient size becomes metastable with respect to its vapor at separations below a critical drying distance D_c .¹⁻⁴ The thermodynamics and kinetics of confinement induced evaporation have continued to receive much attention as they are believed to underlie hydrophobic self-assembly.⁴⁻⁷ In addition, such transitions are suspected to have significant biophysical consequences, underlying the function of membrane bound proteins such as ion-channels^{8,9} and G-protein coupled receptors,¹⁰ both of which are common drug targets due to their role in signaling.

A common model for probing the fundamental physics of hydrophobic evaporation consists of two parallel $L \times L$ hydrophobic plates separated by a distance D , immersed in a bath of liquid water at fixed temperature and chemical potential.^{3,4} The confined $\sim L^2 D$ region is an open system coupled thermodynamically to the surrounding liquid bath. One can

formulate expressions for the grand potential Ω (i.e., the appropriate thermodynamic potential for an open system) of the confined liquid Ω_l and vapor Ω_v at a given separation. The separation such that $\Omega_l(D) = \Omega_v(D)$ provides an estimate of D_c , and for water confined between flexible plates, it is given by

$$D_c = -\frac{2\gamma_{vl} \cos \theta}{\Delta p[1 + \phi]} + \frac{\Delta p \Delta V + \gamma_{vl} \Delta A_{vl} - U_{strain}}{L^2 \Delta p[1 + \phi]}, \quad (1)$$

where the first term on the right-hand side is the estimate for perfectly rigid plates² and the second term on the right-hand side is a modification that accounts for deformations that occur upon evaporation between flexible plates.¹¹ γ_{vl} is the vapor/liquid interfacial tension, Δp is the pressure difference between the liquid bath and the confined vapor, θ is the contact angle of water on the hydrophobic substrate, and $\phi = \frac{4\gamma_{vl}}{L\Delta p}$. For the terms that account for plate deformation, ΔV is the volume that becomes available to the surrounding liquid due to deformation, ΔA_{vl} is the corresponding reduction in vapor/liquid interfacial area, and U_{strain} is the strain energy in the plates.¹¹

For nanoscale plates at ambient conditions, $\phi \gg 1$, as the thermodynamic penalty of forming a vapor/liquid interface far outweighs the increase in bulk free energy. Note that such conditions are relevant to most biophysical applications. In the $\phi \gg 1$ regime, Eq. (1) reduces to

$$D_c = -\frac{L \cos \theta}{2} + \frac{\Delta A_{vl}}{8L}, \quad (2)$$

where the above expression is for the specific example of a linear elastic material, in which case the work of the loads inducing deformation is equal to twice the strain energy (i.e., $2U_{strain} = \Delta p \Delta V + \gamma_{vl} \Delta A_{vl}$).¹² For perfectly rigid materials (i.e., having infinite capacity to withstand deformations under

^{a)}Author to whom correspondence should be addressed: pdebene@princeton.edu

load), $\frac{\Delta A_{vl}}{8L} = 0$. Despite being a macroscopic theory, the above expression, in the rigid limit, has repeatedly been shown to be quantitative.¹³⁻¹⁵ In addition, the flexible modification is positive (i.e., for a linear elastic material: $\Delta p\Delta V + \gamma_{vl}\Delta A_{vl} - U_{strain} = U_{strain} > 0$),¹¹ meaning that flexibility promotes evaporation with respect to otherwise identical rigid plates, a prediction that has recently been verified by us via computer simulations.¹⁶

In addition to informing equilibrium phase behavior, macroscopic thermodynamic arguments (i.e., continuum arguments) are used to interpret the kinetics of evaporation via classical nucleation theory, which posits that the probability of forming an embryo of the stable phase can be related to the reversible work of its formation W .¹⁷ The transition rate is then related to the reversible work of forming an embryo of sufficient size n^* associated with the transition state, called the critical nucleus

$$rate \sim \exp\left[-\frac{W(n^*)}{kT}\right], \quad (3)$$

where kT is the thermal energy. Accordingly, the dependence of $\log(rate)$ upon a given parameter provides information regarding how the free energy barrier scales with that parameter.

For water in hydrophobic confinement, the classical picture is that a gap-spanning cylindrical tube of sufficient radius r_c promotes nucleation.^{18,19} Continuum thermodynamic arguments estimating the reversible work required to form a tube of size r_c lead to

$$\Delta\Omega_{evap}^* = \frac{\pi\gamma_{vl}D^2}{2} + 2\pi\tau D + \frac{2\pi\tau^2}{\gamma_{vl}}, \quad (4)$$

where τ is the line tension, which provides the thermodynamic cost of forming a three-phase contact line.^{14,19} Depending on the relative values of the separation-dependent terms, one expects a quadratic or linear scaling of the barrier with separation. In addition, without a dramatic change in γ_{vl} or τ , Ω_{evap}^* is a continuous, differentiable function of separation. Doubts regarding the applicability of Eq. (4) have largely been limited to the shape of the critical nucleus as it has been noted that the tubes tend to resemble an hour-glass rather than a perfect cylinder.^{4,20-22} In addition, there is some debate over whether the barrier to evaporation is in fact a tube of sufficient radius.^{2,15,16,19,23} However, we have found, by direct observation, that evaporation in nanoscale hydrophobic confinement indeed requires the formation of a tube of sufficient size in order to cross the nucleation barrier.¹⁶

While versions of Eq. (4) have been invoked for some time,^{4,24} relatively few studies have evaluated the accuracy of the scaling suggested by Eq. (4). The earliest test is credited to Luzar,²⁵ who employed 2D lattice gas simulations in solvophobic confinement in conjunction with umbrella sampling to estimate the scaling of Ω_{evap}^* with D and found that $\Omega_{evap}^* \propto D^{1.9}$, a result within error of recovering a quadratic relation. Xu and Molinero²⁶ calculated the barriers to evaporation of the coarse-grained (mW) model of water²⁷ between hydrophobic disks directly from the water content probability distribution and found good agreement with a fit $\Omega_{evap}^* = c(D - 2\delta)^2$, where δ accounts for the distance between the center of mass

of the plate and the closest water molecules, and c is a constant [estimated as $\frac{\pi\gamma_{vl}}{2}$ in Eq. (4)]. Sharma and Debenedetti¹⁹ computed the rates of evaporation of the extended simple point charge (SPC/E) model of water²⁸ between hydrophobic plates using forward flux sampling (FFS),^{29,30} reported linear scaling of $\log(rate)$ versus D , and rationalized the results by suggesting a dominant role of line tension.

Here we revisit our previously employed model system¹⁶ and calculate the rate of evaporation and free energy profiles as a function of separation. The system contains two 3×3 nm² hydrophobic plates immersed in a bath of SPC/E water²⁸ simulated at 298 K and 1 atm. Each plate is composed of three layers of atomic sites, where each nearest neighbor interacts through a harmonic spring with strength K . Tuning K adjusts the overall flexibility of the plates. A more detailed description can be found in Ref. 16. While our previous work sought to elucidate how material flexibility affects the thermodynamics and kinetics of nanoscale hydrophobic evaporation and condensation, the present work provides more detailed calculations to assess the separation dependence of the rate, free energy barriers, and free energy difference between confined liquid and vapor and evaluate their agreement with the macroscopic theories summarized above.

Figure 1 shows the rate versus separation for two different flexibilities, calculated via forward flux sampling.²⁹ Both $K = 1500$ and $1000 \frac{\text{kcal}}{\text{mole } \text{\AA}^2}$ were considered in our previous study¹⁶ but separations were limited to $D = 12.00, 12.50,$ and 13.00 \AA. Here, we have extended the rate calculations below 12.00 \AA and performed additional calculations between 12.00 and 12.50 \AA. We also performed repeat calculations at $D = 11.75$ and 12.00 \AA for $K = 1500$.

Neither flexibility exhibits a simple $\log(rate)$ versus D relationship for the range of separations considered. At higher separation, both curves are linear, consistent with Eq. (4) in the limit of dominant line tension. However, at lower separation, both curves appear to show a “break” that separates two limiting behaviors. The $K = 1500$ plates exhibit a nearly

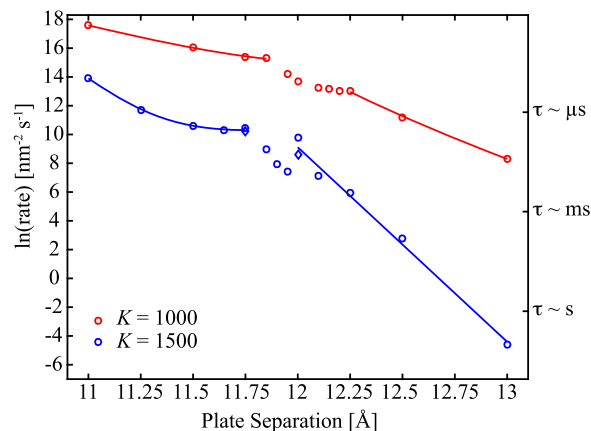


FIG. 1. Evaporation rates as a function of plate separation for two different flexibilities ($K [=] \frac{\text{kcal}}{\text{mole } \text{\AA}^2}$). The right-hand axis indicates the characteristic time scales of evaporation. The lines are guides to the eye and illustrate a break between two limiting behaviors, and the two diamonds along the $K = 1500$ curve are repeat calculations at $D = 11.75$ and 12.00 \AA.

discontinuous response between $D = 11.95$ and 12.00 Å. Following the break, the curve appears quadratic but exhibits positive curvature. For the $K = 1000$ plates, the break corresponds to a region of positive curvature, with both sides of the break exhibiting linear behavior. Without an abrupt change in the surface or line tension, such features are inconsistent with the predictions of Eq. (4). It has been suggested that part of the free energy profile is consistent with classical nucleation theory if one allows these physical parameters to depend on separation.¹⁵ However, both curves contain regions of positive curvature, in conflict with the predictions of Eq. (4), even with varying physical constants.

To formulate Eqs. (1), (2), and (4), the confined fluid is considered a continuum. However, it is well known that fluids in nanoscale confinement will exhibit layering to accommodate the geometric constraint. Surface force apparatus measurements show evidence of oscillatory forces below about 1.5 nm separations due to water layering, with a periodicity corresponding to the diameter of a water molecule.³¹ Indeed, layering has been observed in numerous simulation studies and is expected to be important for the diffusive association of hydrophobic objects.^{7,32} Here we provide a structural characterization of the aqueous film that suggests that subtle features can impact the rate of evaporation.

Figure 2 shows the average density profile of water between the above-described plates, for a range of plate separations for the $K = 1500$ and 1000 plates, shifted such that $z = 0$ corresponds to the midpoint between the two plates. This average is performed over the expanse of the plates in the x - y plane for bin widths of 0.05 Å in the z -direction. Thus, features in the x - y plane such as local cavities, which are important for the kinetics of evaporation,^{15,16} are averaged out. In addition, such an analysis lacks any information about molecular orientation that may be important for a network fluid like water.

As expected, the density profile exhibits peaks and valleys associated with layering of the confined fluid. Recall that these represent density probabilities, and the water molecules remain highly mobile (i.e., liquid-like). At larger plate separations, there are three peaks corresponding to three water layers. As the plates are brought closer together, the middle peak weakens and eventually inverts to minimum, as the liquid

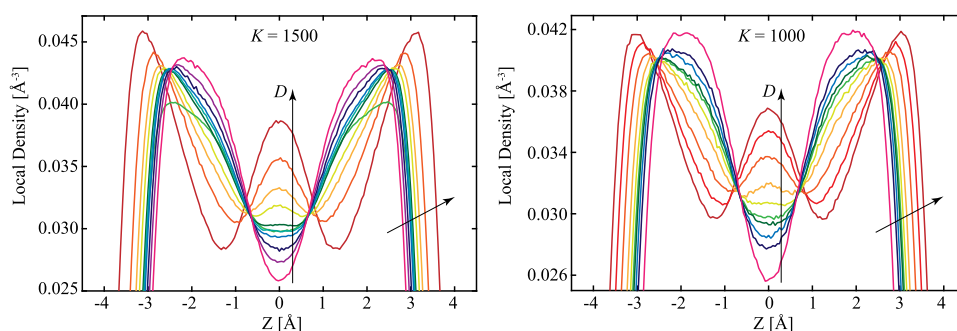


FIG. 2. Local density of water in hydrophobic confinement for a variety of separations D for both the $K = 1500$ and $K = 1000$ plates. A transition between a trilayer to bilayer occurs for both flexibilities in rough correspondence to the break in the rate of evaporation. The $K = 1500$ plot includes separations 11.50, 11.65, 11.75, 11.85, 11.90, 11.95, 12.00, 12.10, 12.25, 12.50, and 13.00 Å. The $K = 1000$ plot includes separations 11.50, 11.75, 11.85, 11.95, 12.00, 12.10, 12.25, 12.50, 12.75, and 13.00 Å.

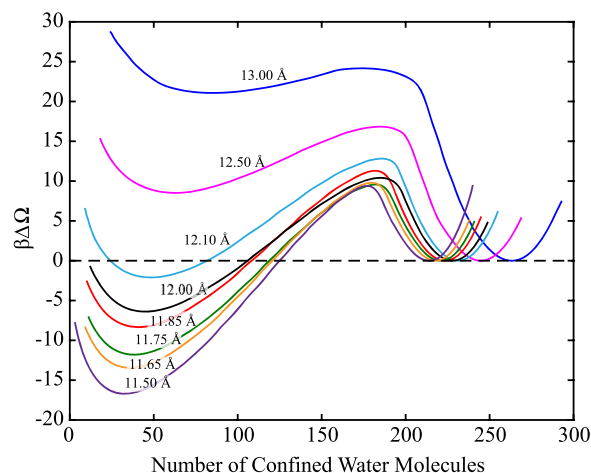


FIG. 3. Free energy calculations for the $K = 1500$ plates for different separations. The figure displays the full free-energy profile projected onto the number water molecules confined between the plates; the liquid basin is fixed at 0 for all separations. The profiles show that the barrier to evaporation does not decrease monotonically below 12.00 Å. However, the vapor becomes progressively stabilized with respect to the liquid as separation decreases, suggesting that non-monotonicity in the barrier is solely a kinetic effect.

film transitions from a trilayer to bilayer. This transition occurs between $D = 11.95$ and 12.00 Å for the $K = 1500$ plates and between $D = 12.00$ and 12.10 Å for the $K = 1000$ plates. In both cases, the transition between tri- and bi-layer is in rough correspondence to the location of the “break” in the rate, suggesting that the latter is a result of a structural transition in the liquid film. The film must rupture in order to evaporate.^{15,16} Thus, it appears reasonable that structural details of the film have implications for the kinetics of evaporation.

For the $K = 1500$ plates, we have computed a selection of free energy profiles projected onto the number of confined water molecules between the plates (Fig. 3). These profiles are computed by performing FFS in both directions to obtain the stationary distribution of the FFS order parameter,³³ which in this case is the number of confined water molecules. The liquid basin is shifted to $\beta\Delta\Omega = 0$ for all separations. As implied by the rate calculations (Fig. 1), the free energy barrier to evaporation becomes a non-monotonic function of separation below 12 Å. From these calculations, it is clear that a non-monotonic barrier to evaporation is largely consistent with

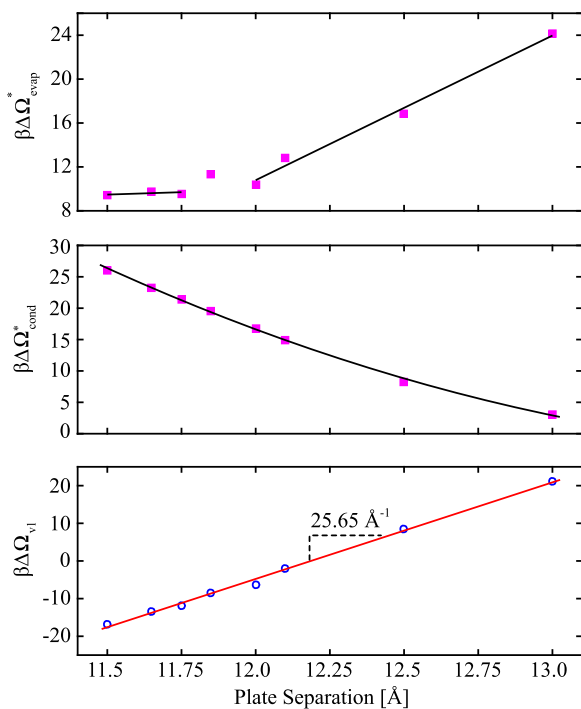


FIG. 4. Quantities extracted from the free energy profiles: barrier to evaporation (top), barrier to condensation (middle), and free energy difference between vapor and liquid (bottom). The top plot is consistent with the rate calculations and displays a break between two different trends. The middle plot shows that the barrier to condensation is well described by a quadratic fit, in agreement with the scaling suggested by nucleation theory. The bottom plot shows that that free energy difference between the confined vapor and liquid is linear, in agreement with macroscopic thermodynamic theory. The slope, predicted to be $4\gamma_{vl}L/kT$, provides a surface tension of 0.072 J/m^2 , suggesting quantitative agreement with the macroscopic theory.

impeded kinetics, as the vapor basin monotonically descends with separation. The top plot in Fig. 4 displays the barrier to evaporation $\beta\Delta\Omega_{\text{evap}}^*$ versus separation. The curve shows linear behavior at larger separation and then flattens at lower separation, with a jump in between.

For the confined vapor to condense, the interface with the surrounding liquid must spontaneously collapse inward to allow the surrounding liquid to penetrate the confined region. As this interface collapses, the barrier to condensation is likewise a gap-spanning tube of sufficient size. Since condensation is the reverse of evaporation, the barrier to condensation $\beta\Delta\Omega_{\text{cond}}^*$ is simply $\beta\Delta\Omega_{\text{evap}}^* - \beta\Delta\Omega_{\text{vl}}$, where $\beta\Delta\Omega_{\text{vl}}$ is the free energy difference between the vapor and liquid. Since $\beta\Delta\Omega_{\text{vl}}$ is linear in D ,¹¹ $\beta\Delta\Omega_{\text{cond}}^*$ is quadratic with the same leading coefficient as in Eq. (4).

Figure 4 (middle) plots $\beta\Delta\Omega_{\text{cond}}^*$ versus separation. While the free energy barrier to evaporation appears to be coupled to the structure of the liquid film, the free energy barrier to condensation $\Delta\Omega_{\text{cond}}^*$ is well described by a quadratic fit, in agreement with the predictions of classical nucleation theory (best quadratic fit has $R^2 = 0.999$; best linear fit has $R^2 = 0.987$). However, if one attempts to estimate the surface tension through the coefficient to D^2 in Eq. (4), one obtains $\gamma_{vl} = 1.0 \text{ J/m}^2$, a fairly poor agreement. Thus, while the trends of classical nucleation are preserved for condensation, they do not appear to be quantitative.

The macroscopic thermodynamic theory employed to estimate D_c predicts a linear relationship between $\Delta\Omega_{\text{vl}}$ and D , with slope $4\gamma_{vl}L$. Note that while $\Delta\Omega_{\text{vl}}$ is a function of flexibility (i.e., K), the slope is given by $\left(\frac{\partial\Delta\Omega_{\text{vl}}}{\partial D}\right)_K = 4\gamma_{vl}L$,¹¹ which is K -independent. Our computed $\Delta\Omega_{\text{vl}}$ are well described by a line with a slope of 25.65 kT/\AA (Fig. 4, bottom). Solving for γ_{vl} yields an estimate of the surface tension of 0.072 J/m^2 , a value roughly 13% higher than SPC/E's surface tension,³⁴ a very reasonable agreement. Note that we have typically defined L as the distance between atomic centers of sites on opposite edges of the plate. To obtain this estimate of γ_{vl} , two Lennard-Jones distances $2\sigma = 0.6566 \text{ nm}$ characterizing the wall-water interactions were added to the plate length (making it effectively 3.6555 nm), in a spirit similar to the modification of D by Xu and Molinero.²⁶ It appears that the arguments that result in Eqs. (1) and (2) provide a quantitative description of the thermodynamics of water in nanoscale hydrophobic confinement. We note that a linear relationship between $\Delta\Omega_{\text{vl}}$ and D has recently been reported for the case of water confined between perfectly rigid, hydrophobic disks.³⁵

The results presented here suggest that subtle structural features of confined aqueous films can dramatically impact the kinetics of hydrophobically induced evaporation. While our previous work¹⁶ suggests that the barrier to evaporation is a gap-spanning tube of sufficient size, invoking macroscopic arguments to formulate a nucleation theory appears to have little predictive value. Thus, caution is warranted in relying on macroscopic theories to formulate simple design rules within the context of the kinetics of hydrophobic nanoscale evaporation. However, the thermodynamics of evaporation/condensation are fairly well described by macroscopic thermodynamic arguments. In addition, the kinetics of condensation qualitatively follow the predictions of classical nucleation theory. The difference between the behavior of evaporation and condensation may be a result of an out-sized role of interfacial density fluctuations^{15,16,36} and possibly shape fluctuations of the vapor tube²⁴ in evaporation.

Y.E.A. is grateful to Nyssa Emerson for figure preparation assistance. P.G.D. gratefully acknowledges support from the National Science Foundation (Grant Nos. CHE-1213343 and CBET-1263565). Computations were performed at the Terascale Infrastructure for Groundbreaking Research in Engineering and Science at Princeton University.

¹A. Wallqvist and B. J. Berne, *J. Phys. Chem.* **99**, 2893 (1995).

²K. Lum and A. Luzar, *Phys. Rev. E* **56**, R6283 (1997).

³C. A. Cerdeirina, P. G. Debenedetti, P. J. Rossky, and N. Giovambattista, *J. Phys. Chem. Lett.* **2**, 1000 (2011).

⁴X. Huang, C. J. Margulis, and B. J. Berne, *Proc. Natl. Acad. Sci. U. S. A.* **100**, 11953 (2003).

⁵D. Chandler, *Nature* **437**, 640 (2005).

⁶J. Y. Li, J. A. Morrone, and B. J. Berne, *J. Phys. Chem. B* **116**, 11537 (2012).

⁷J. A. Morrone, J. Li, and B. J. Berne, *J. Phys. Chem. B* **116**, 378 (2012).

⁸A. Anishkin and S. Sukharev, *Biophys. J.* **86**, 2883 (2004).

⁹F. Q. Zhu and G. Hummer, *Proc. Natl. Acad. Sci. U. S. A.* **107**, 19814 (2010).

¹⁰S. G. Yuan, S. Filipek, K. Palczewski, and H. Vogel, *Nat. Commun.* **5**, 4733 (2014).

¹¹Y. E. Altabet and P. G. Debenedetti, *J. Chem. Phys.* **141**, 18C531 (2014).

¹²L. D. Landau and E. M. Lifshitz, *Theory of Elasticity* (Pergamon, Oxford, 1986).

¹³H. S. Ashbaugh, *J. Chem. Phys.* **139**, 064702 (2013).

- ¹⁴S. Sharma and P. G. Debenedetti, *J. Phys. Chem. B* **116**, 13282 (2012).
- ¹⁵R. C. Remsing, E. Xi, S. Vembanur, S. Sharma, P. G. Debenedetti, S. Garde, and A. J. Patel, *Proc. Natl. Acad. Sci. U. S. A.* **112**, 8181 (2015).
- ¹⁶Y. E. Altabet, A. Haji-Akbari, and P. G. Debenedetti, *Proc. Natl. Acad. Sci. U. S. A.* **114**, E2548 (2017).
- ¹⁷P. G. Debenedetti, *Metastable Liquids: Concepts and Principles* (Princeton University Press, Princeton, 1996).
- ¹⁸V. S. Yushchenko, V. V. Yaminsky, and E. D. Shchukin, *J. Colloid Interface Sci.* **96**, 307 (1983).
- ¹⁹S. Sharma and P. G. Debenedetti, *Proc. Natl. Acad. Sci. U. S. A.* **109**, 4365 (2012).
- ²⁰K. Lum and D. Chandler, *Int. J. Thermophys.* **19**, 845 (1998).
- ²¹A. Luzar and K. Leung, *J. Chem. Phys.* **113**, 5836 (2000).
- ²²B. J. Berne, J. D. Weeks, and R. H. Zhou, *Annu. Rev. Phys. Chem.* **60**, 85 (2009).
- ²³P. G. Bolhuis and D. Chandler, *J. Chem. Phys.* **113**, 8154 (2000).
- ²⁴K. Leung and A. Luzar, *J. Chem. Phys.* **113**, 5845 (2000).
- ²⁵A. Luzar, *J. Phys. Chem. B* **108**, 19859 (2004).
- ²⁶L. M. Xu and V. Molinero, *J. Phys. Chem. B* **114**, 7320 (2010).
- ²⁷V. Molinero and E. B. Moore, *J. Phys. Chem. B* **113**, 4008 (2009).
- ²⁸H. J. C. Berendsen, J. R. Grigera, and T. P. Straatsma, *J. Phys. Chem.* **91**, 6269 (1987).
- ²⁹R. J. Allen, P. B. Warren, and P. R. ten Wolde, *Phys. Rev. Lett.* **94**, 018104 (2005).
- ³⁰R. J. Allen, C. Valeriani, and P. R. ten Wolde, *J. Phys.: Condens. Matter* **21**, 463102 (2009).
- ³¹J. N. Israelachvili and R. M. Pashley, *Nature* **306**, 249 (1983).
- ³²J. Mondal, J. A. Morrone, and B. J. Berne, *Proc. Natl. Acad. Sci. U. S. A.* **110**, 13277 (2013).
- ³³C. Valeriani, R. J. Allen, M. J. Morelli, D. Frenkel, and P. R. ten Wolde, *J. Chem. Phys.* **127**, 114109 (2007).
- ³⁴C. Vega and E. de Miguel, *J. Chem. Phys.* **126**(10), 154707 (2007).
- ³⁵B. S. Jabes, J. Driskill, D. Vanzo, D. Bratko, and A. Luzar, *J. Phys. Chem. C* **121**, 13144 (2017).
- ³⁶A. J. Patel, P. Varilly, and D. Chandler, *J. Phys. Chem. B* **114**, 1632 (2010).